Numerical Simulation of Regular Waves onto a Vertical Circular Cylinder

Zhenghao Liu[*], Decheng Wan[‡]

State Key Laboratory of Ocean Engineering, School of Naval Architecture, Ocean and Civil Engineering,
Shanghai Jiao Tong University, Collaborative Innovation Center for Advanced Ship and Deep-Sea Exploration,
Shanghai 200240, China
[*]Presenting author: xiakee@sjtu.edu.cn
[‡]Corresponding author: dcwan@sjtu.edu.cn
http://dcwan.sjtu.edu.cn

Abstract

Wave run-up phenomenon is of great significance during the design of a fixed or floating structure. In this work, the wave run-up on a truncated surface-piercing circular cylinder is investigated using a numerical wave tank. The numerical simulations are carried out by the in-house CFD solver naoe-FOAM-SJTU which is developed on the open source platform OpenFOAM. The volume of fluid (VOF) method is applied to capture the free surface. The surface elevation around the cylinder is probed by a series of wave gauges and analyzed using the Fourier analysis. The response amplitude operates (RAOs) of surface elevation are presented and compared with experimental data. Reasonable agreement shows the present solver is capable to investigate the wave run-up on a cylinder. The local surface elevation around the cylinder, the wave force and the scattered wave field around the cylinder is also investigated in detail.

Keywords: wave run-up; truncated vertical cylinder; naoe-FOAM-SJTU solver; surface elevation

Introduction

Offshore structures such as Spars, semi-submersibles and tension leg platforms (TLP) have been widely applied in ocean engineering. Wave run-up on the columns of the structures can be relatively large and even causes green water on deck in severe environment. Generally, wave run-up height is defined as the maximum vertical wave elevation to the still water surface. Significant nonlinear wave-structure interactions can be observed during the wave run-up process. The accurate prediction of wave run-up is of great importance for the air-gap design of offshore structures. Numerous researchers have done experimental, theoretical and numerical studies on wave run-up onto piles, sloped beaches and columns of both fixed and floating offshore structures.

Various experimental investigations of wave run-up on vertical cylinders have previously been performed. Galvin and Hallermeier (1972) experimentally studied the wave run-up on a cylindrical column for the first time [1]. A series of wave gauges were mounted near the column to obtain the distribution of free surface around the column. It was found that when the waves pass through the vertical column, two important factors will affect the wave run-up effect: 1) scattering effect due to wave-structure interaction; 2) viscous dissipation effect at the column wake region. Chakrabarti and Tam (1975) conducted a series of model tests to investigate the regular waves onto a large-scale cylinder [2]. The incident wave steepness kA is 0.03~0.19 and the scattering parameter kr is 0.34~1.55, respectively. Their work was focused on the wave run-up phenomenon and the effect of incident wave angle on the distribution of the cylinder surface pressure, while the free surface around the cylinder was

not discussed. Morris-Thomas et al. (2002) investigated the effect of wave steepness and the scattering parameter on the wave run-up on a fixed cylinder in a towing tank [3]. Nielsen (2003) firstly studied the effect of cross-sectional shape on the wave run-up and free surface of cylinders [4]. Compared with circular cylinder, stronger nonlinear interaction can be found for circular-like cylinder. Systematic model tests were conducted in Shanghai Jiaotong University to investigate the effect of aspect ratio, cross-sectional shape, wave parameters and current on wave run-up phenomenon in 2010.

Besides experimental research on wave run-up, the nonlinear wave-structure interaction phenomenon has been studied by numerous researchers through theoretical methods. Generally, the theoretical methods are based on potential theory in which an idealized fluid domain is assumed. The Laplace equation is solved with applied boundary conditions to yield a velocity potential. The free-surface elevation around the column can be obtained by application of the unsteady Bernoulli equation and velocity potential at the free-surface position. In the early days, the approximate results of wave run-up on a single cylinder according to first- and second-order potential flow theory [5][6]. Trulsen and Teigen (2002) developed fully nonlinear numerical wave tanks (NWT) to investigate nonlinear interaction between wave and a truncated cylinder, and compared the predicted results with experimental data [7]. They found the effects of viscosity may take account for the discrepancies between the theoretical method and experiment. Similar researches can be found in [8]. Morris-Thomas and Thiagarajan (2004) adopted the linear diffraction theory and the commercial software WAMIT to predict the wave run-up around a cylinder [9]. They suggested that linear diffraction theory is insufficient for wave run-up estimation. This confirms conclusions made by previous authors. The second-order harmonic components predicted by WAMIT show reasonable estimates of wave run-up when the scattering parameter is small.

With the rapid development of computer technology during the last several decades, computational fluid dynamics (CFD) method has been widely applied in ocean engineering field. Previous numerical simulations based on CFD have also been performed on wave run-up problems. Based on the open source platform OpenFOAM, Cao and Wan (2014, 2015, 2017) simulated the regular and solitary waves on to a circular cylinder, and the comparison of numerical results of wave run-up and experimental data showed the reasonable agreement [10]-[12]. Donald G Danmeier et al. [13] used the ComFLOW software to simulate the wave run-up around a semi-submersible platform. Sun et al. [14] used a both potential flow solver DIFFRACT and a full CFD solver OpenFOAM to investigate nonlinear interactions between regular waves and a single truncated circular column. The predicted free surface elevation around the column and the wave forces were analyzed and compared with experimental data.

To investigate wave run-up, the ITTC committee organized several studies, including experimental and numerical researches in 2013. The results of a series of model tests for a truncated circular column in regular waves at MARINTEK and MOERI are used in the ITTC benchmark study [15]. The time histories of surface elevations and wave forces were provided.

The objective of the present work is to investigate the wave run-up on a surface-piercing circular cylinder. The computations in this paper are performed with the in-house CFD solver naoe-FOAM-SJTU, which is developed based on the open source code OpenFOAM. The numerical results of the free surface elevation around the column and the wave forces are presented and compared with experiments performed at MOERI. The details information of wave run-up around cylinder will be given and discussed. The results show that the present approach can be an alternative tool to deal with nonlinear wave-structure interactions.

Numerical methods

naoe-FOAM-SJTU solver

The CFD solver naoe-FOAM-SJTU is designed for computing viscous flows around ships and ocean structures [16-20] and mainly composed of a dynamic deforming mesh module, a 6DoF motion module, a velocity inlet wave-making module and a mooring system module.

In present study, the incompressible unsteady Reynolds averaged Navier-Stokes (URANS) equations are adopted as the governing equations, and can be written as follows:

$$\nabla \cdot \boldsymbol{U} = 0 \tag{1}$$

$$\frac{\partial \rho \boldsymbol{U}}{\partial t} + \nabla \cdot (\rho (\boldsymbol{U} - \boldsymbol{U}_g) \boldsymbol{U}) = -\nabla p_d - \boldsymbol{g} \cdot x \nabla \rho + \nabla \cdot (\mu_{eff} \nabla \boldsymbol{U}) + (\nabla \boldsymbol{U}) \cdot \nabla \mu_{eff} + f_\sigma + f_s \tag{2}$$

where $\boldsymbol{U}$ and $\boldsymbol{U}_g$ are the velocity field and the velocity of grid nodes, respectively. p_d is the dynamic pressure and p is the total pressure, ρ is the mixed density of the two phases water and air. μ_{eff} is the effective dynamic viscosity, in which ν and ν_t are kinematic viscosity and eddy viscosity, respectively. f_σ is the surface tension, which impacts the free surface. f_s is a source term, added to generate the sponge layer for wave absorbing.

Capture of Free Surface

The free surface of the two-phase flow is captured by the volume of fluid (VOF) method [21] with artificial bounded compression techniques. The method is based on a volume fraction α which can control numerical diffusion and capture the interface with high resolution. The volume fraction function can be determined by solving a transport equation:

$$\frac{\partial \alpha}{\partial t} + \nabla \cdot [(\boldsymbol{U} - \boldsymbol{U}_g) \alpha] + \nabla \cdot [\boldsymbol{U}_r (1 - \alpha) \alpha] = 0 \tag{3}$$

The first two terms on the left-hand side of Eq. (3) stand for traditional volume of fluid transport equation while the third term represents the artificial compression term. The velocity field $\boldsymbol{U}_r$ compressing the interface is computed at cell faces by the maximum velocity magnitude at the interface region:

$$U_{r,f} = n_f \min \left\{ C_\alpha \frac{|\phi|}{|s_f|}, \max \left(\frac{|\phi|}{|s_f|} \right) \right\} \tag{4}$$

where φ is face volume flux; C_α is a compression coefficient controlling the magnitude of compression, in this paper it is chosen to be 1.0. Larger value will increase the compression of the interface, leading to larger detrimental velocity gradients around the interface. The compression term only works on the interface without affecting the numerical computation out of the transition layer due to term $(1-\alpha)\alpha$.

Different phases are marked using volume fraction α which indicates the relative proportion of fluid in each cell, it is defined as Eq. (5). For an interface cell, the value of volume fraction α is between 0 and 1, representing it contains both water and air.

$$\begin{cases} \alpha=0 & \text{air} \\ \alpha=1 & \text{water} \\ 0<\alpha<1 & \text{interface} \end{cases} \tag{5}$$

In physical domain, the density of fluid ρ and the dynamic viscosity μ can be obtained by a weighted value based on the volume fraction α:

$$\rho = \alpha\rho_1 + (1-\alpha)\rho_2 \tag{6}$$

$$\mu = \alpha\mu_1 + (1-\alpha)\mu_2 \tag{7}$$

Where ρ_1 and ρ_2 denote the density of water and air, μ_1 and μ_2 denote the viscosity coefficient of water and air, respectively.

Wave Generation and Damping

Our naoe-FOAM-SJTU solver includes a wave generation and damping module. To generate the Stokes first deep water wave, the inlet boundary conditions are set as follows:

$$\eta = a\cos(\mathbf{k}\cdot\mathbf{x} - \omega_e t + \delta) \tag{8}$$

$$u = U_0 + a\omega e^{kz}\cos(\mathbf{k}\cdot\mathbf{x} - \omega t + \delta) \tag{9}$$

$$v = a\omega e^{kz}\cos\beta\cos(\mathbf{k}\cdot\mathbf{x} - \omega t + \delta) \tag{10}$$

$$w = a\omega e^{kz}\sin\beta\sin(\mathbf{k}\cdot\mathbf{x} - \omega t + \delta) \tag{11}$$

Where ζ is transient wave elevation, a, ω and $\mathbf{k}$ are wave amplitude, wave frequency and wave number, respectively. $\mathbf{U_0}$ is hull speed.

To avoid wave reflection, a sponge layer is setup at the outlet of the computational domain. The term of f_s is introduced into Eq. (2) for absorption of waves and defined as:

$$f_s(x) = \begin{cases} -\rho\alpha_s(\dfrac{x-x_s}{L_s})^2(U-U_{ref}) \\ 0 \end{cases} \tag{12}$$

Where in which, ρ is the water density. The α_s is an artificial viscosity coefficient controlling the intensity of the sponge layer. The x_s is the coordinate of the start position of the sponge layer and L_s is the length of the sponge layer. The source term f_s has no effects on the domain out of the sponge layer.

Discretization schemes

The RANS and VOF transport equations are discretized by finite volume method (FVM). Van Leer scheme is applied for VOF equation in OpenFOAM. The PIMPLE (merged PISO-SIMPLE) algorithm is used to solve the coupled equation of velocity and pressure. The convection terms are solved by a second-order TVD limited linear scheme, and the diffusion terms are approximated by a second-order central difference scheme.

Computational model and test conditions

Computational model

To simulate wave run-up on a truncated surface-piercing column, the cylinder model at full scale from MOERI is selected in numerical simulation. The radius of the cylinder is $R = 8.0$ m, and the draft is 24.0 m. A series of wave probes in both experiment and numerical simulation are shown in Figure 1, and the corresponding location are given in Table 1. The distances between inner circle and outer circle are 0.2063 m and 8 m, respectively.
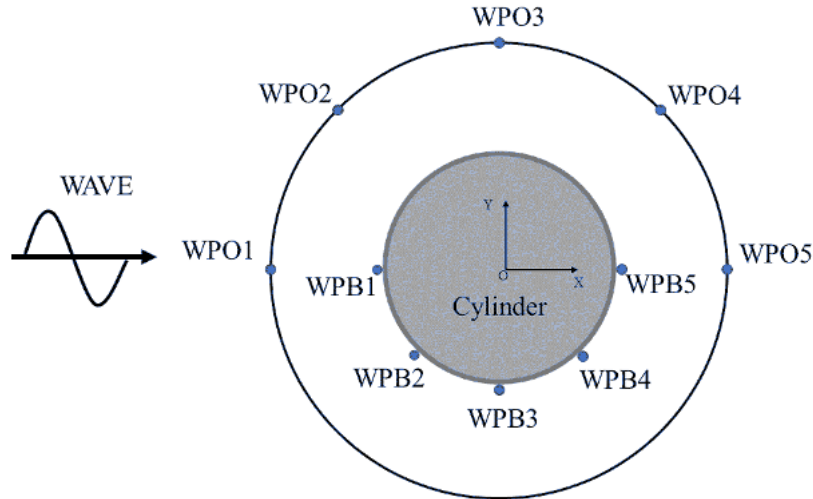
Figure 1 Layout of wave probes

Table 1 Location of wave probes

Inner circle	x (m)	y (m)	Outer circle	x (m)	y (m)
WPB1	-8.2063	0.0000	WPO1	-16.0000	0.0000
WPB2	-5.8027	-5.8027	WPO2	-11.3137	-11.3137
WPB3	0.0000	-8.2063	WPO3	0.0000	16.0000
WPB4	5.8027	-5.8027	WPO4	11.3137	11.3137
WPB5	8.2063	0.0000	WPO5	16.0000	0.0000

Figure 2 shows the arrangement of computational domain. The domain extends to $-2L < x < 3L$, $-L < y < L$, $-L < z < 0.5L$. Where L represents the wave length. The water depth is set as L. The length of sponge length is L, starting from $x = 2L$. The vertical cylinder is fixed in the center of the wave tank.
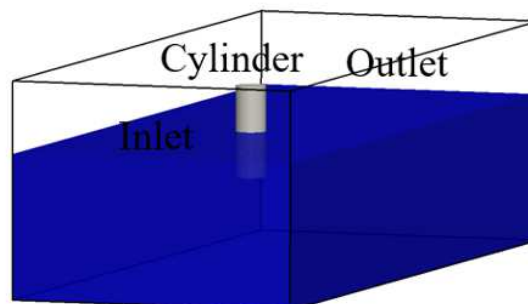
Figure 2 Computational domain

The computational mesh is shown in Figure 3. About 70 grids per wavelength and 20 per wave height are applied. The total grid number is about 1.7 million. To make it easy to converge in each time step, the interface Courant number was controlled to be under 0.3. The

time step is 0.001s in each case. The boundary conditions are as follows: Velocity inlet is adopted. Zero-Gradient condition is applied at the outlet. The no-slip boundary condition is imposed on the cylinder. The symmetry boundary condition is applied to the side walls.
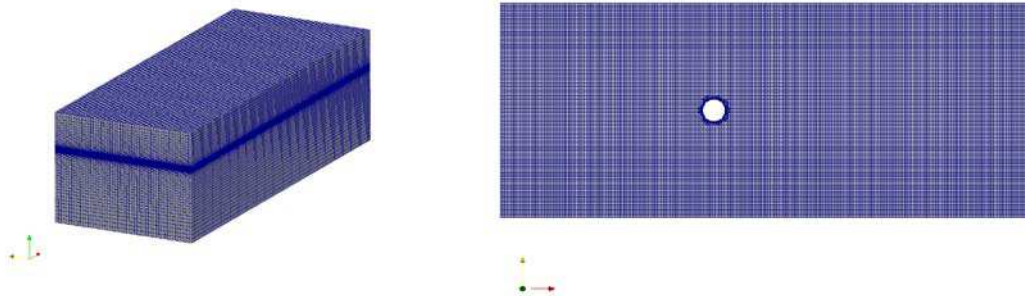
Figure 3 Mesh of computational domain

Test conditions

The incident wave conditions were set up according to the benchmark study conditions proposed by the 27th ITTC committee. The Stokes first order deep water wave is applied in the present work. Two wave periods (T = 7s, 9s) have been investigated. Three steepness parameters (H/L = 1/30, 1/16 and 1/10) were simulated for each wave period, where H is the wave height and L is the wave length. Another parameter in our analysis is the scattering parameter $k_0 r$, where k_0 ($k_0 = 2\pi/L$) is the wave number. Details of the wave conditions are listed in Table2.

Table 2 Wave conditions

	T = 7 s			T = 9 s		
H/L	L(m)	D/L	H (m)	L(m)	D/L	H (m)
1/30			2.548			4.212
1/16	76.44	0.21	4.777	126.36	0.13	7.898
1/10			7.644			12.636

Results and discussion

RAOs of surface elevations

The response amplitude operates (RAOs) are effectively transfer functions used to determine the effect of wave on the ocean structures. The obtained time histories of free surface elevation are generally analyzed to acquire the RAOs using the Fourier analysis. The acquired RAOs of free surface elevations at ten wave probe locations from our CFD simulation are compared with the experimental data from MOERI. The RAOs of free surface elevations from potential flow solver DIFFRACT [14] are also adopted in this work. Figure 4 shows the comparisons of the RAOs of surface elevation near the cylinder at WPB3 and WPB4 for the condition wave period T = 7s and H/L =1/30, 1/16, 1/10. As shown in Figure 4(a), for small wave steepness condition, both the CFD results and DIFFRACT results agree well with the experimental data at WPB3. As the steepness increases, the CFD solver can give more accurate prediction than the potential flow theory. This is more obvious for WPB4 in Figure 4(b), for the H/L = 1/10 condition, the CFD solver can give a much better agreement with the experimental data. This may be the strong nonlinear interactions at the downstream location WPB4. Reasonable agreement between the CFD results and experimental data implies that the present solver is capable to predict the wave run-up on a truncated cylinder.
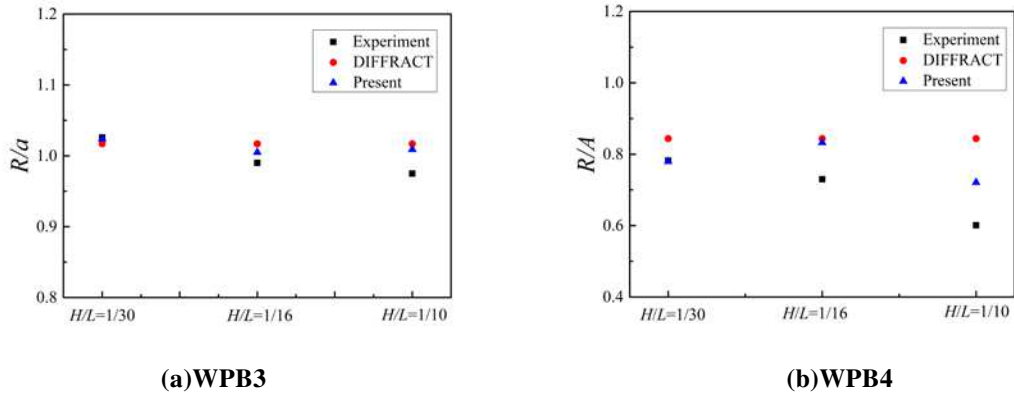
(a)WPB3   (b)WPB4

Figure 4 Comparisons of RAOs of surface elevations for *T* = 7s

Time histories of wave probes

For the wave period *T* = 7s condition, time histories of the free surface elevation obtained from our CFD simulation are shown in Figure 5 (inner circle probes) and Figure 6 (outer circle probes). As can be seen from Figure 5, the wave probe in front of the cylinder reaches the largest wave amplitude in any wave height condition. This may due to the wave-structure interaction in front of the cylinder. When the wave crest reaches the cylinder, the water runs up vertically along the cylinder. The surface elevation at WPB1 is about two times than the incident wave amplitude. The surface elevation at the downstream quarter point WPB4 is the smallest, and secondary crests can be found for steeper waves (*H/L* = 16 and 1/10). This may imply strong nonlinear interaction at this location. After passing the sides of the column, the incident wave encounters and interferes with each other, resulting free wave flows backwards in the upstream direction and overlaps with the incident wave. Thus, the secondary crest can be observed. Similar trends can be found for outer circle wave probes, as shown in Figure 6. However, the discrepancies for these wave probes is reduced compared with the inner circle ones. The secondary crests at WPO4 is not so obvious as WPB4 near the cylinder.

For the wave period *T* = 9s condition, time histories of the free surface elevation are shown in Figure 7 (inner circle probes) and Figure 8 (outer circle probes). The missing of surface elevation data at WPO4 for *H/L* = 1/16 condition is caused by inappropriate wave probe setup in numerical simulation. Secondary wave crest can also be found at WPB4 in steep waves (*H/L* = 16 and 1/10).
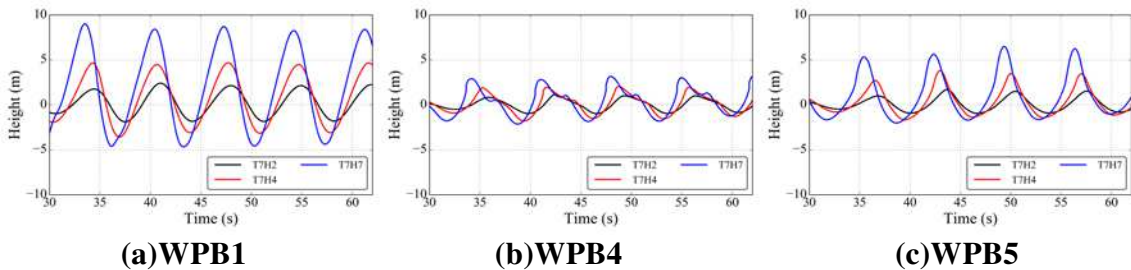
(a)WPB1   (b)WPB4   (c)WPB5

Figure 5 Time series of surface elevation for inner circle wave probes for *T* = 7s
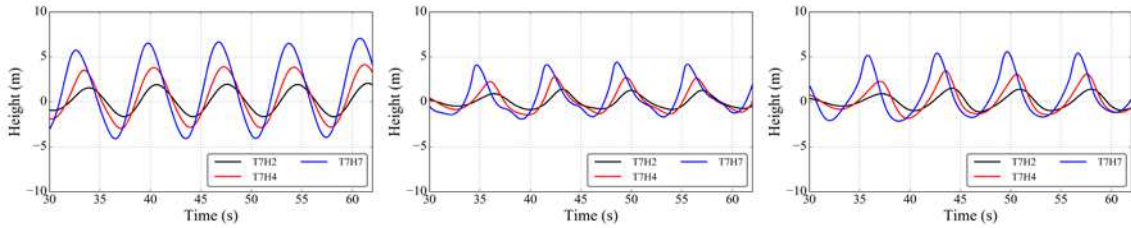
(a)WPO1　　　　　　　(b)WPO4　　　　　　　(c)WPO5

Figure 6 Time series of surface elevation for outer circle wave probes for *T* = 7s
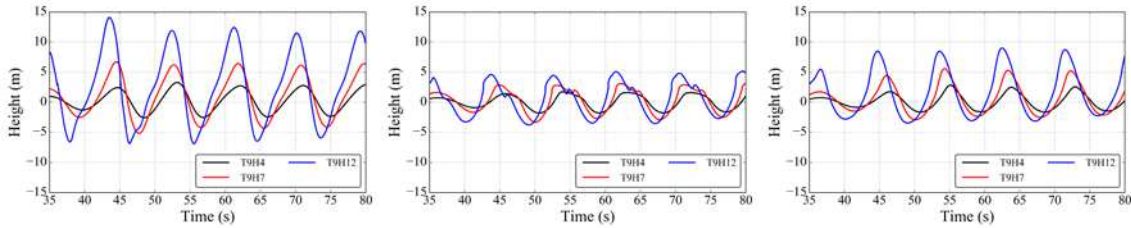
(a)WPB1　　　　　　　(b)WPB4　　　　　　　(c)WPB5

Figure 7 Time series of surface elevation for inner circle wave probes for *T* = 9s
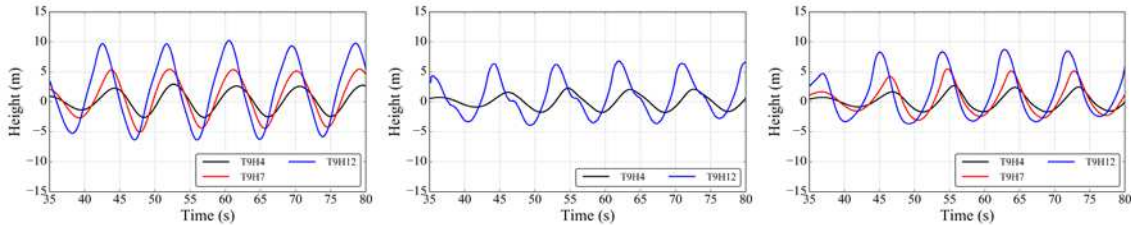
(a)WPO1　　　　　　　(b)WPO4　　　　　　　(c)WPO5

Figure 8 Time series of surface elevation for outer circle wave probes for *T* = 9s

Time histories of wave forces

Figure 9 and Figure 10 show the time histories of horizonal wave force for *T* = 7s and *T* = 9s, respectively. The horizonal wave force increases with the wave height. The nonlinearity in wave force is not as strong as surface elevation. This is because the local nonlinear effects are integrated out when computing the force, while the surface elevation show the original local nonlinearity of wave run-up the cylinder. So it is essential to study the local free surface near the cylinder.
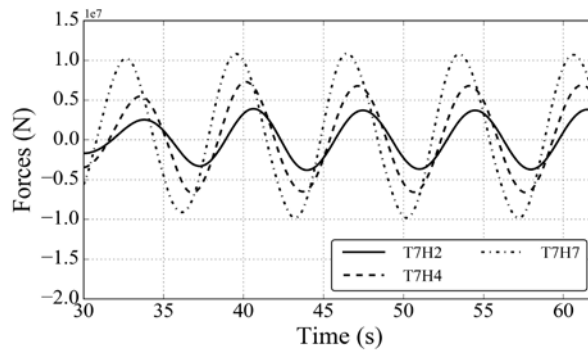
Figure 9 Time series of horizonal wave force for *T* = 7s
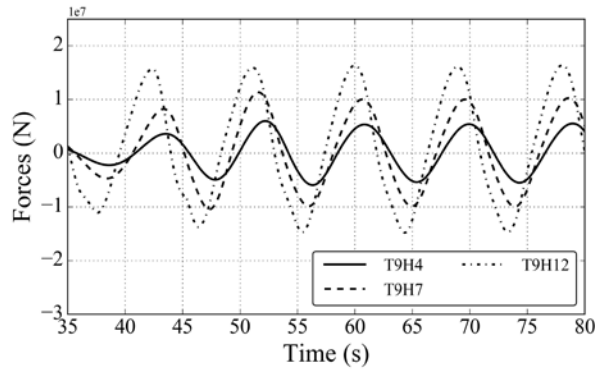
Figure 10 Time series of horizonal wave force for *T* = 9s

Scattered wave field around the cylinder

Figure 11 shows the local free surface around the cylinder for wave at *T* = 7s and *H*/*L* =1/10. The wave diffraction field around the cylinder can be clearly seen. When the wave crest approaches the cylinder, the water is blocked in front of the cylinder and concentric wave field (type1) can be observed. This is specified by Swan and Sheikh (2015) [22]. Then the water bypasses the side of the cylinder, the non-concentric wave field (type2) is developed at the downstream shoulders. This may induce strong nonlinearity at the shoulders of the cylinder. When the water encounters and overlaps at the rear side of cylinder, the run-up phenomenon can also be observed.
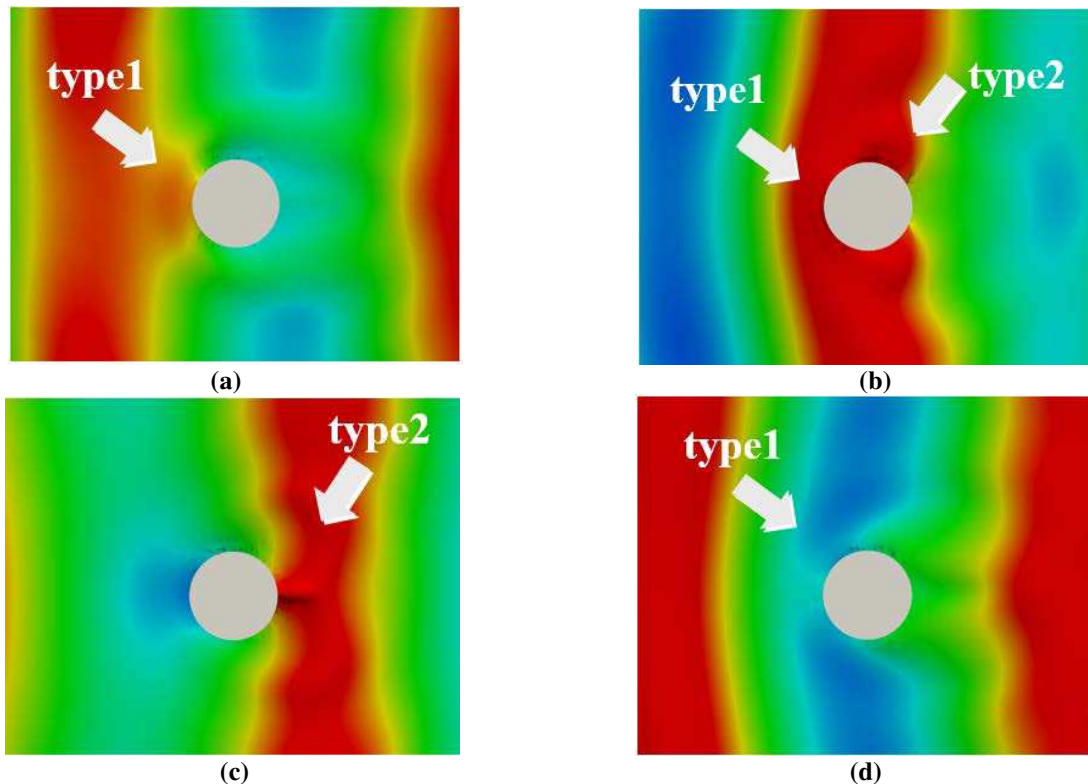
Figure 11 Local free surface around the cylinder

Figure 12 shows the dynamic pressure contours on the cylinder surface at the moment that the wave crest encounters the cylinder surface for wave at *T* = 7s and *H*/*L* =1/30, 1/16, 1/10. The dynamic pressure increases with the increasing wave height. For wave at *T* = 7s and *H*/*L* =

1/10 condition, the maximum dynamic pressure in the front of the cylinder can been found. For each case, the maximum dynamic pressure of the cylinder is close to the free surface.

(a)*H/L* = 1/30   (b) *H/L* = 1/16   (c) *H/L* = 1/10
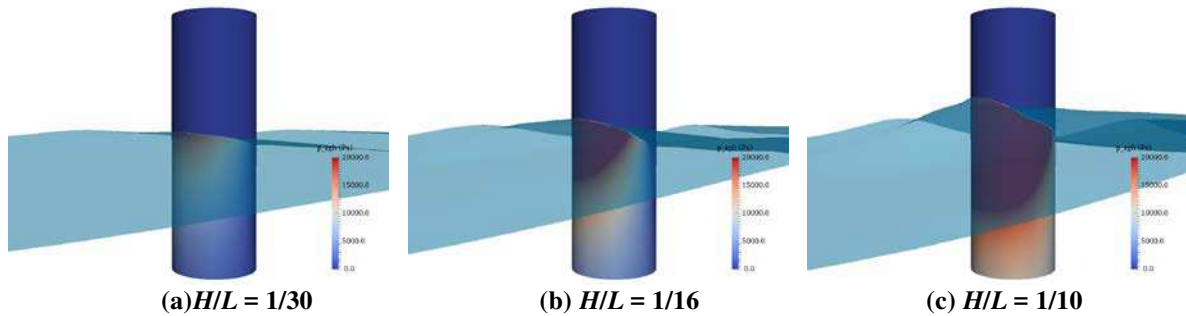
Figure 12 Dynamic pressure the cylinder

Conclusions

In this paper, numerical simulation of the wave run-up on a fixed surface-piercing cylinder in regular waves are performed by the in-house naoe-FOAM-SJTU solver. Two wave periods (*T* = 7s and 9s) and three wave heights (*H/L* =1/30, 1/16, 1/10) are conducted to investigate the wave run-up phenomenon. The predicted RAOs of local surface elevation are compared with the experimental data and good agreement can be acquired even at the strong nonlinear interaction location, where secondary crests can be observed for steeper waves. This can be caused by the overlap between the backward wave from rear part and the incident wave. Concentric and non-concentric wave fields around the cylinder can be captured by the present CFD solver. The surface elevation around the cylinder and the dynamic pressure increases with the increasing wave height. This study shows the capability of the present solver to investigate the wave run-up on a fixed cylinder. Further work should be focused on high-order harmonic and detailed flow information around the cylinder.

Acknowledgements

References

[1]   Galvin, C. J., Hallermeier, R. J. (1972) Wave runup on vertical cylinders, *Coastal Engineering* **1**, 1955-1974.
[2]   Chakrabarti, S. K., Tam, W. A. (1975) Wave height distribution around a vertical cylinder, *Journal of Waterways, Harbours and Coastal Engineering* **101**, 225-230.
[3]   Morris-Thomas, M. T., Thiagarajan, K., Krokstad, J. R. (2002) An experimental investigation of wave steepness and cylinder slenderness effects on wave run-up, In *Proceedings of 21st International Conference on Offshore Mechanics and Arctic Engineering*, OMAE2002-28050.
[4]   Nielsen, F. G. (2003) Comparative study on airgap under floating platforms and run-up along platform columns, *Marine Structures* **16**, 97-134.
[5]   Havelock, T. H. (1940) The pressure of water waves upon a fixed obstacle, In Proceedings of the Royal Society of London A: Mathematical, Physical and Engineering Sciences **175**, 409-421.
[6]   Hunt, J. N., Baddour, R. E. (1981) The diffraction of a nonlinear progressive wave by a vertical cylinder, *Quarterly Journal of Mechanics and Applied Machematics* **34**, 69-88.

[7]   Trulsen, K., Teigen, P. (2002) Wave scattering around a vertical cylinder: fully nonlinear potential flow calculations compared with low order perturbation results and experiment, In *Proceedings of 21st International Conference on Offshore Mechanics and Arctic Engineering*, OMAE2002-28173.

[8]   Teigen, P., Niedzwecki, J. M. (2003) Wave diffraction effects and runup around multicolumn structure, In *Proceedings of 13th International Offshore and Polar Engineering Conference*, 137-144.

[9]   Morris-Thomas, M. T., Thiagarajan, k. (2004) The run-up on a cylinder in progressive surface gravity waves: harmonic components, *Applied Ocean Research* **26**, 98-113.

[10] Cao, H. J., Wan, D. C. (2014) Development of multidirectional nonlinear numerical wave tank by naoe-FOAM-SJTU solver. *International Journal of Ocean System Engineering* **4**, 52-59.

[11] Cao, H. J., Wan, D. C. (2017) Benchmark computations of wave run-up on single cylinder and four cylinders by naoe-FOAM-SJTU solver, *Applied Ocean Research* **65**, 327-337.

[12] Cao, H. J., Wan, D. C. (2015) RANS-VOF solver for solitary wave run-up on a circular cylinder, *China Ocean Engineering* **29**, 183-196.

[13] Danmeier, D. G., Seah, R. K., Finnigan, T., Roddier, D., Aubault, A., Vache, M., Imamura, J. T. (2008) Validation of wave run-up calculation methods for a gravity based structure. In *Proceedings of the ASME 27th International Conference on Offshore Mechanics and Arctic Engineering*, OMAE2008-57625.

[14] Sun, L., Zang, J., Chen, L., Taylor, R. E., Taylor, P. H. (2016) Regular waves onto a truncated circular column: A comparison of experiments and simulations, *Applied Ocean Research* **59**, 650-662.

[15] Kristiansen, T., Baarholm, R., & Stansberg, C. T. (2004) Validation of second-order analysis in predicting diffracted wave elevation around a vertical circular cylinder, In *Proceedings of 14th International Offshore and Polar Engineering Conference*, 342-349.

[16] Shen, Z. R., Wan, D. C., Carrica, P. M. (2015) Dynamic overset grids in OpenFOAM with application to KCS self-propulsion and maneuvering. *Ocean Engineering* **108**, 287-306.

[17] Wang, J. H., Wan, D. C. (2016) Numerical simulation of pure yaw motion using dynamic overset grid technology. *Chinese Journal of Hydrodynamics* **31**, 567-574.

[18] Ye, H. X., Wan, D. C. (2017) Benchmark computations for flows around a stationary cylinder with high Reynolds numbers by RANS-overset grid approach, *Applied Ocean Research* **65**, 315-326.

[19] Shen, Z. R., Wan, D. C. (2016) An irregular wave generating approach based on naoe-FOAM-SJTU solver, *China Ocean Engineering* **30**, 177-192.

[20] Liu, Z. H., Wan, D. C. (2016) Numerical simulation of green water on S-175 containership, In *Proceedings of the Second Conference of Global Chinese Scholars on Hydrodynamics*, 815-821.

[21] Hirt, C. W., Nichols, B. D. (1981) Volume of fluid (VOF) method for the dynamics of free boundaries. *Journal of Computational Physics* **39**, 201-225.

[22] Swan, C., Sheikh, R. (2015) The interaction between steep waves and a surface-piercing column, *Philosophical Transactions of the Royal Society of London A* **373**, 20140114.